Ann. Geophys., 32, 689–704, 2014
www.ann-geophys.net/32/689/2014/
doi:10.5194/angeo-32-689-2014

Annales Geophysicae
Open Access

Magnetospheric magnetic field modelling for the 2011 and 2012 HST Saturn aurora campaigns – implications for auroral source regions

E. S. Belenkaya[1], S. W. H. Cowley[2], C. J. Meredith[2], J. D. Nichols[2], V. V. Kalegaev[1], I. I. Alexeev[1], O. G. Barinov[1], W. O. Barinova[1], and M. S. Blokhina[1]

[1]Lomonosov Moscow State University, Skobeltsyn Institute of Nuclear Physics, 1(2), Leninskie Gory, GSP-1, Moscow 119991, Russian Federation
[2]Department of Physics & Astronomy, University of Leicester, Leicester LE1 7RH, UK

Correspondence to: E. S. Belenkaya (elena@dec1.sinp.msu.ru)

Received: 6 November 2013 – Revised: 14 May 2014 – Accepted: 20 May 2014 – Published: 27 June 2014

Abstract. A unique set of images of Saturn's northern polar UV aurora was obtained by the Hubble Space Telescope in 2011 and 2012 at times when the Cassini spacecraft was located in the solar wind just upstream of Saturn's bow shock. This rare situation provides an opportunity to use the Kronian paraboloid magnetic field model to examine source locations of the bright auroral features by mapping them along field lines into the magnetosphere, taking account of the interplanetary magnetic field (IMF) measured near simultaneously by Cassini. It is found that the persistent dawn arc maps to closed field lines in the dawn to noon sector, with an equatorward edge generally located in the inner part of the ring current, typically at ~ 7 Saturn radii (R_S) near dawn, and a poleward edge that maps variously between the centre of the ring current and beyond its outer edge at $\sim 15\,R_S$, depending on the latitudinal width of the arc. This location, together with a lack of response in properties to the concurrent IMF, suggests a principal connection with ring-current and nightside processes. The higher-latitude patchy auroras observed intermittently near to noon and at later local times extending towards dusk are instead found to straddle the model open–closed field boundary, thus mapping along field lines to the dayside outer magnetosphere and magnetopause. These emissions, which occur preferentially for northward IMF directions, are thus likely associated with reconnection and open-flux production at the magnetopause. One image for southward IMF also exhibits a prominent patch of very high latitude emissions extending poleward of patchy dawn arc emissions in the pre-noon sector. This is found to lie centrally within the region of open model field lines, suggesting an origin in the current system associated with lobe reconnection, similar to that observed in the terrestrial magnetosphere for northward IMF.

Keywords. Magnetospheric physics (planetary magnetospheres)

1 Introduction

While the principal mechanism driving the auroras at Earth is the interaction with the solar wind, for Jupiter and Saturn the most significant roles are played by internal processes, specifically the internal sources of plasma from moons that orbit within the magnetosphere and rapid planetary rotation (see, e.g. the reviews by Krupp et al., 2004 and Mitchell et al., 2009a, and references therein). Nevertheless, this does not preclude the solar wind interaction from playing an important role in outer magnetosphere dynamics at the giant planets; furthermore, it is known, in particular, that bright auroral emissions extend to very high latitudes in the dawn sector at Saturn in response to strong magnetospheric compressions by the solar wind (Prangé et al., 2004; Clarke et al., 2005, 2009). In addition, structured dayside auroral features observed in the post-noon sector have been interpreted as the signatures of time-dependent reconnection and open-flux production at the dayside magnetopause, similar to "flux transfer events" at Earth (Radioti et al., 2011, 2013; Badman et al., 2013; Meredith et al., 2014).

In this context we note that magnetopause reconnection may differ somewhat between Earth and Saturn, due to the differing physical conditions occurring at the boundary. In particular, flow-shear effects between the magnetosheath and sub-corotating magnetospheric plasma may suppress reconnection in the pre-noon sector of strong shear (Owen and Cowley, 1987; Desroche et al., 2013), while pressure gradient effects across the boundary may restrict reconnection to regions where the internal and external fields are closely anti-parallel (Swisdak et al., 2003; Masters et al., 2012). Nevertheless, auroral observations show that the open flux in Saturn's dark "polar cap" mapping to the tail varies considerably with time over the range ∼ 10–50 GWb (e.g. Grodent et al., 2005), implying typical reconnection (open-flux production) rates ∼ 50–100 kV, comparable to estimates based on simple scaling of empirical Earth values (Jackman et al., 2004; Badman et al., 2005). Indeed, in the auroral events studied by Radioti et al. (2011), the expansion in open-flux observed implies mean reconnection rates of ∼ 400 kV over an interval of several hours.

In this paper we continue to investigate the origins of Saturn's auroras using the Kronian paraboloid magnetospheric magnetic field model to map bright auroral features along field lines into the magnetosphere using a new set of auroral images. This model, introduced by Alexeev et al. (2006) and Belenkaya et al. (2006a), has most recently been used by Belenkaya et al. (2013) to magnetically map bright auroral forms from Saturn's southern ionosphere to both the magnetospheric equatorial plane and the northern ionosphere. This model includes the planetary field, a ring current and tail field, and screening currents flowing on a paraboloid magnetopause, together with a uniform field representing a partially penetrating interplanetary magnetic field (IMF). Model modifications introduced by Belenkaya et al. (2013) include use of the Burton et al. (2010) axial multi-pole model of the internal planetary magnetic field, together with a spheroidal form for the ionospheric level where the auroral emission intensity is taken to be at its maximum. It was shown in previous work that such mapping is controlled by the IMF penetrating into the magnetosphere (Belenkaya et al., 2007, 2008, 2010, 2011). However, situations where we know the IMF vector at the times of Saturn auroral images occur very rarely. Belenkaya et al. (2013) worked with only two Hubble Space Telescope (HST) images, obtained in 2008, one of which occurred for northward IMF and the other for southward. This work therefore represented only an initial step in identifying the regions magnetically conjugate to Saturn's auroras, but did not allow general conclusions to be drawn.

Here we work with an expanded set of eight recent images of Saturn's northern auroras obtained during the 2011 and 2012 HST campaigns, when the Cassini spacecraft was simultaneously located in the solar wind just upstream of Saturn's bow shock measuring the IMF. In a parallel study of these images, Meredith et al. (2014) found no clear IMF response in the dawn emissions, while patchy auroras observed at higher latitudes in the noon to dusk sector were found to occur for northward but not for southward IMF, thus suggesting a connection with reconnection-related processes at the magnetopause as discussed previously by Radioti et al. (2011, 2013) and Badman et al. (2013). In addition, a prominent patch of polar emissions observed in one image for southward IMF was suggested to be due to high-latitude "lobe reconnection" between the IMF and open tail flux tubes poleward of the dayside cusp (e.g. Cowley, 1981). Following the work of Belenkaya et al. (2013), here we use the modified paraboloid model to map bright auroral features in these images along model field lines into the magnetosphere using the measured IMF as input. Since the images were obtained only ∼ 1.5–2.5 years after Saturn equinox (August 2009), their coverage is confined principally to dayside auroral emissions, such that we are concerned mainly with field line mapping in the dayside magnetosphere. Our results are found to be compatible with the physical suggestions of Meredith et al. (2014).

2 Observational data

We begin in Fig. 1 by showing the Cassini IMF data employed in this paper, where Fig. 1a and b show intervals encompassing the HST imaging "visits" examined here, undertaken during the 2011 and 2012 Saturn campaigns, respectively (days 90–97 inclusive of 2011 and 2012). The top panels in each plot show the field strength on a logarithmic scale, while the panels beneath show the x, y, and z field components in Kronian solar–magnetospheric (KSM) coordinates. (In the KSM system, x points toward the Sun, the x–z plane contains the planet's spin/magnetic axis, and y completes the right-hand set pointing towards dusk.) The KSM coordinates of the spacecraft (R_S) are given at day markers at the bottom of each plot, together with the spacecraft radial distance R. (R_S is Saturn's 1 bar equatorial radius equal to 60 268 km.) In both cases Cassini was moving outward in the post-noon sector at the beginning of each interval, passing through apoapsis in the near-equatorial pre-dusk sector within each plot (see the R values), on revolutions (Revs) 146/147 during the 2011 campaign and 163/164 on the 2012 campaign. (Cassini Rev numbers are defined from apoapsis to apoapsis.)

During the interval shown in Fig. 1a for the 2011 campaign, the spacecraft was principally located in the solar wind measuring the IMF, but with occasional transitions into the magnetosheath. The latter are readily discerned in the field magnitude panel as intervals of elevated field strength having very sharp boundaries, as the spacecraft crossed the bow shock. The centre time of each of the four ∼ 44 min HST imaging intervals discussed here, corrected for the Saturn–Earth light travel time, are shown by the vertical black dashed lines, marked with an image identifier (H1–H4) at the top of the panel. It can be seen that the spacecraft was located in the solar wind (rather than the magnetosheath) at the time of each

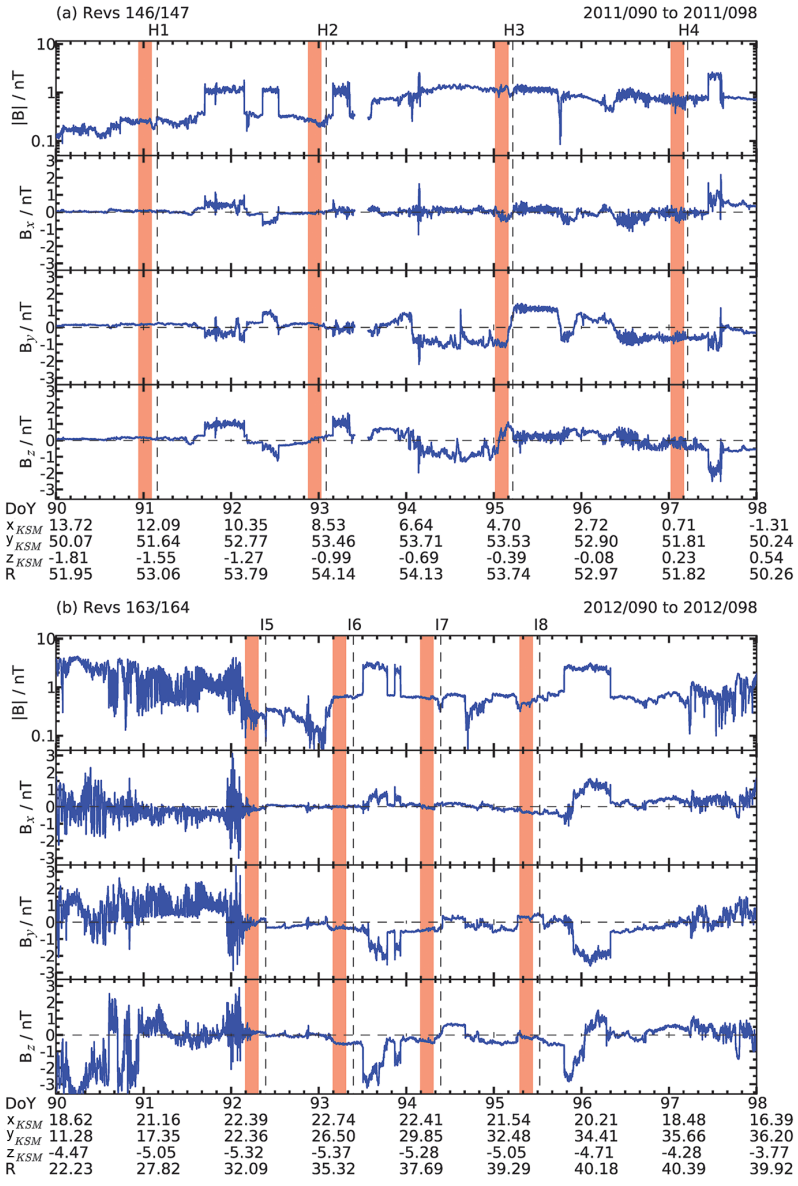

Figure 1. Plots showing Cassini magnetic field data encompassing HST imaging intervals during **(a)** the 2011 Saturn campaign (Revs 146/147), and **(b)** the 2012 campaign (Revs 163/164). Eight days of data are shown in each case (days 90–97 inclusive of 2011 and 2012), with spacecraft position data (KSM coordinates) and radial distance (R_S) being given at day boundaries at the bottom of each plot. The top panel of each plot shows the total field strength on a logarithmic scale (nT), while the three panels beneath show the x, y, and z field components (nT), also in KSM. The dashed vertical lines show the Saturn centre time of four ∼44 min HST imaging intervals in each panel, for which Cassini had been located continuously in the solar wind for at least several hours previously. Image identifiers are shown at the top of each plot. The associated pink stripes show the lagged 3 h intervals over which these IMF values have been averaged to generate a characteristic IMF (and standard deviation) for each image interval, as given in Table 1.

image, and had been for a substantial prior interval. The vertical pink bands show the lagged 3 h intervals over which the IMF has been averaged to generate an overall value, as will be discussed further below. It can be seen, for example, that IMF B_y was consistently positive during these intervals for H1 and H2, and consistently negative for H3 and H4, while IMF B_z was mainly positive for H1–H3, and mainly negative for H4.

Similarly in Fig. 1b for the 2012 campaign, the spacecraft was initially intermittently located within the magnetosphere on day 90 (negative B_z intervals), consistently in the magnetosheath on day 91, and passed out across the bow shock into the solar wind early on day 92. Thereafter the spacecraft was located principally in the solar wind, though again with occasional intervals in the magnetosheath, clearly indicated by elevated fields with sharp boundaries. The centre times of four

HST imaging intervals, and associated lagged IMF averaging intervals, are again shown by the vertical black dashed lines and pink bands, respectively, with image identifiers (I5–I8) shown at the top of the plot. The IMF averaging intervals are again seen to be located continuously in the solar wind, with IMF B_y consistently negative for I6 and I7, consistently positive for I8, and near zero for I5, while IMF B_z was mainly positive for I5, and negative for I6 to I8. A range of differing IMF conditions is thus seen to have been present during these imaging intervals.

The corresponding HST images of the northern dayside auroras are shown in Figs. 2a–5a for the 2011 campaign (H1–H4), and in Figs. 6a–9a for the 2012 campaign (I5–I8). In each case all image sub-frames over the imaging interval (termed a "visit") have been co-added to maximise the signal-to-noise, and have been projected onto a surface 1100 km above the 1 bar planetary reference spheroid where the auroral emission maximises (Gérard et al., 2009). Image resolution near noon is $\sim$ 400 km east–west, but $\sim$ 1000 km north–south due to the oblique view. White dotted circles and radial lines show 10° latitude and 2 h local time (LT) lines, respectively, with noon at the bottom and dawn to the left. The images have been truncated past the dawn–dusk meridian where the data approach the planetary limb, with somewhat better coverage being available for the 2012 images compared with 2011 due to the developing northern spring season at Saturn. The visit identifier is given at the top of each image, together with the date (year-month-day) and image UT centre time (hour:min:sec). These centre times are tabulated in the second column of Table 1, where the third column also gives the "Saturn time" of the image, corrected for light travel from the planet to the HST. A colour-coded intensity (kR) scale is also shown above the images, which is the same for each image so they may be compared directly.

The first image in Fig. 2a is from visit H1, obtained on 1 April 2011 centred at 05:03:51 UT. As in many of these images, but not all, the auroral emission can be divided into three regions, consisting with increasing LT of a dawn arc, a noon spot, and dusk emission. To trace these features into the magnetosphere, we have identified the boundaries of the emissions and have marked them with numbered symbols as shown in the figure, typically taken at intervals of 0.5 h LT, from which field lines have been computed using the field model to be discussed in Sect. 3. The equatorward and poleward boundaries of the dawn arc are shown by light green triangles and dark green squares, respectively, where the boundary is taken to correspond to the appropriate vertex of the symbol. Similarly, the equatorward and poleward boundaries of the dusk arc are shown by violet triangles and brown squares. The point numbers increase from the nightside towards noon along each border. Points on the boundary of the near-noon spot are centred within open red circles. The brown curve over plotted on the image shows the boundary between open and closed field lines computed from the magnetic field model using the KSM components of the IMF measured by Cassini, lagged and averaged as described below.

Examining the other images from the 2011 campaign, it can first be seen that for visit H2 in Fig. 3a (3 April at 03:23:19 UT), the noon spot now lies close to the eastward end of the dawn arc, though at higher latitudes, while only weak vestiges of the dusk emission remains. For H3 in Fig. 4a (5 April at 06:30:29 UT), we see a continuous bright wide auroral oval that shifts to higher latitudes in the post-noon sector, while for H4 in Fig. 5a (7 April at 06:26:11 UT) a latitudinally broad band of auroras spans from beyond the dawn meridian towards noon, extending poleward close to the magnetic/spin pole of the planet itself. Previous studies have shown that such "disturbed" auroral morphologies occur in response to rapid compressions of the magnetosphere by the solar wind (Prangé et al., 2004; Clarke et al., 2005, 2009), possibly resulting in rapid reconnection and open-flux closure in the tail (Cowley et al., 2005).

Turning now to the 2012 campaign images, for visit I5 in Fig. 6a (1 April at 10:47:15 UT) it can be seen that a narrow dawn arc extends into the pre-noon sector, together with a prominent high-latitude spot near noon, while weaker emissions are only present in the post-noon sector past the dusk meridian, taking the form of a narrow arc extending from higher to lower latitudes with increasing LT. The auroras for I6 in Fig. 7a (2 April at 10:48:56 UT) exhibit similar features to visit I5 near dawn and dusk, though the emissions near noon are located at a significantly lower latitude, and could instead represent a continuation of the dawn arc having become somewhat patchy in the pre-noon sector and moving to somewhat higher latitudes. For visit I7 in Fig. 8a (3 April at 10:45:49 UT), we then observe only a broad bright dawn arc extending fully to the noon meridian where it moves to higher latitudes, with no separate noon spot or significant emissions in the post-noon sector to dusk and beyond. For visit I8 in Fig. 9a (4 April at 13:54:13 UT), the dawn arc is once more narrow, and, similar to the case for I6, may extend into patchy forms near noon that move to higher latitudes, marked separately in the figure by dark blue and purple asterisks on the poleward and equatorward borders, respectively. This image also contains a new feature, namely patchy emissions extending over the polar region, principally on the dawn side of the noon–midnight meridian, marked by light blue and orange asterisks. As for visit I7, there are no significant emissions in the post-noon sector at usual oval latitudes in this case. Overall it can be seen that a variety of auroral morphologies exist within this data set, though with a number of common features as well.

We now consider the lagged and averaged values which are used to characterise the IMF during each HST imaging interval, which are employed in the magnetic field modelling discussed in Sect. 3. The minimum lag time relative to the centred "Saturn time" of each image has been estimated by considering the "frozen-in" field propagation delay from the spacecraft to the subsolar bow shock, the

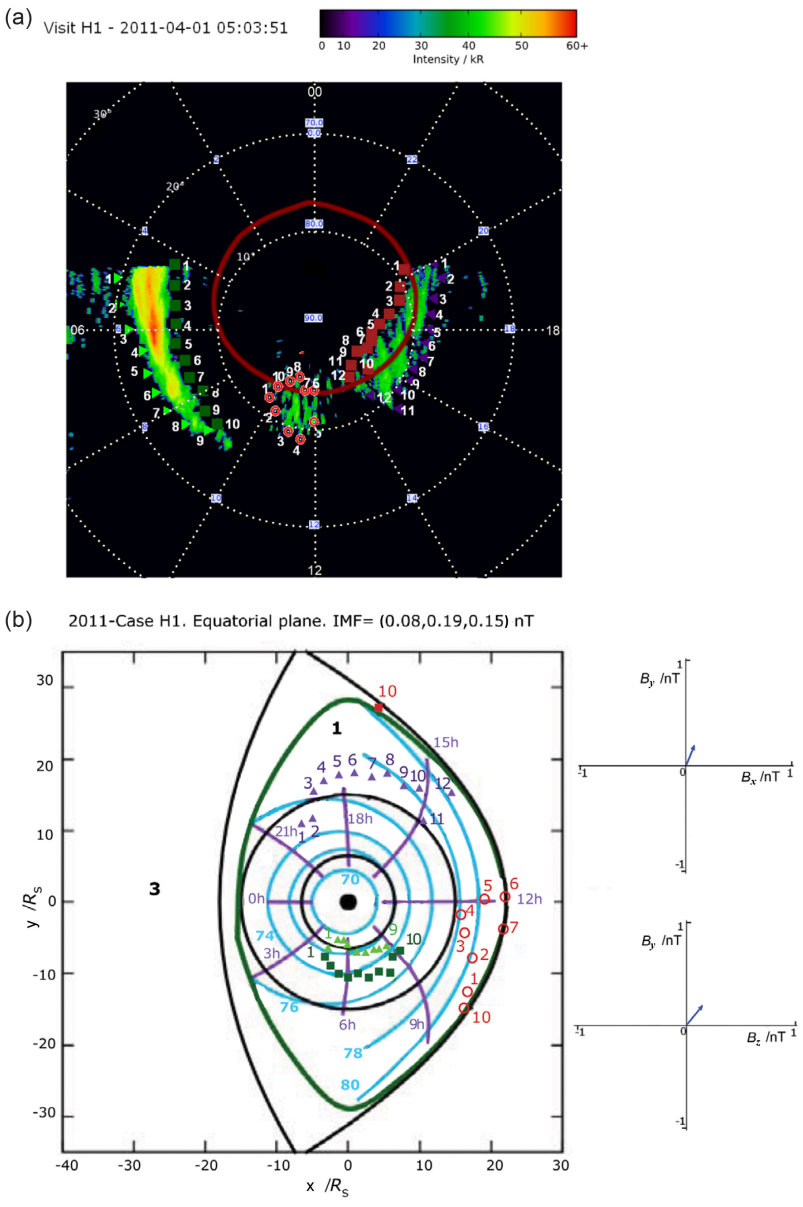

Figure 2. (a) Image of Saturn's northern UV aurora obtained on HST visit H1, co-added over all image sub-frames during the ∼ 44 min imaging interval, shown projected onto a surface 1100 km above the 1 bar reference spheroid. White dotted lines show latitude circles at 10° intervals and radial longitude lines at 2 h LT intervals, with noon at the bottom and dawn to the left. The visit identifier is given above the image, together with the date (year-month-day) and light-propagation corrected UT centre time (h:min:s). An emission intensity (kR) scale is also shown, common to all the images shown. Numbered light green triangles and dark green squares mark the equatorward and poleward borders of the dawn arc, respectively, shown every ∼ 30 min of LT, red circles mark the boundary of the near-noon spot, while blue triangles and brown squares mark the equatorward and poleward borders of the pre-dusk emission. The brown curve shows the model open–closed field boundary, computed using the concurrent IMF vector, derived as described in Sect. 2. **(b)** The KSM equatorial plane of Saturn's magnetosphere, viewed from the north with the Sun to the right. The black curve on the right shows the magnetopause surface, a paraboloid of revolution about the x axis, while the black curve to the left shows the inner edge of the tail current sheet. The black circles show the inner and outer edges of the model ring current. The green line marks the boundary between closed field lines (region 1) and interplanetary lines that have penetrated into the magnetosphere (region 3). Projections of constant latitude circles from the north are shown by the blue lines, marked with the corresponding latitude at 2° intervals. Projections of lines of constant LT at steps of 3 h are shown by violet lines. Boundaries of the auroral forms in **(a)** are shown projected along model field lines to the equatorial plane using the same numbered symbols. The lagged 3 h averaged concurrent IMF vector employed in the model is indicated above the plot, with the vector shown blue being projected into the x–y (upper) and z–y (lower) planes on the right.

Table 1. Centre HST and Saturn times of auroral images, lag times for field averages, and average and RMS deviation KSM field components.

Visit	HST centre time (UT)	Saturn time (UT)	t_1 (h)	t_2 (h)	B_x (nT)	B_x RMS	B_y (nT)	B_y RMS	B_z (nT)	B_z RMS
H1	2011-04-01 05:03:51	2011-04-01 03:52:13	1.552	4.552	0.076	0.022	0.186	0.016	0.154	0.026
H2	2011-04-03 03:23:19	2011-04-03 02:11:41	1.414	4.414	−0.041	0.055	0.173	0.059	0.130	0.064
H3	2011-04-05 06:30:29	2011-04-05 05:18:51	1.250	4.250	−0.283	0.152	−0.933	0.202	0.432	0.401
H4	2011-04-07 06:26:11	2011-04-07 05:14:32	1.091	4.091	−0.154	0.189	−0.588	0.131	−0.147	0.156
I5	2012-04-01 10:47:15	2012-04-01 09:34:29	1.985	4.985	−0.153	0.100	−0.075	0.101	0.153	0.083
I6	2012-04-02 10:48:56	2012-04-02 09:36:12	1.987	4.987	−0.005	0.026	−0.333	0.046	−0.536	0.025
I7	2012-04-03 10:45:49	2012-04-03 09:33:07	1.965	4.965	−0.064	0.057	−0.426	0.050	−0.406	0.058
I8	2012-04-04 13:54:13	2012-04-04 12:41:33	1.916	4.916	−0.340	0.037	0.270	0.057	−0.173	0.057

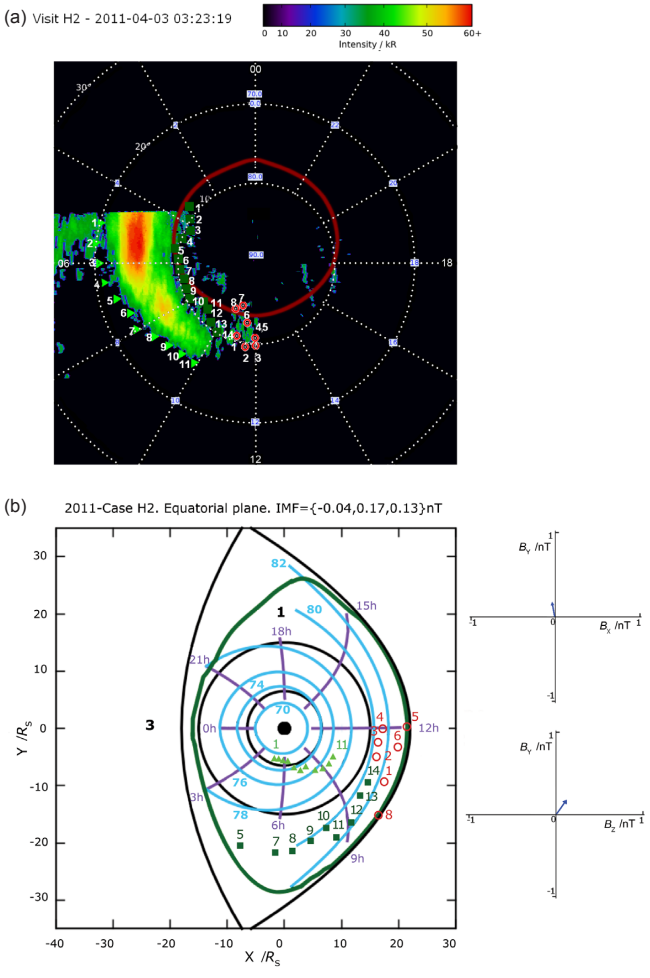

Figure 3. HST image and equatorial mapping for visit H2, in the same format as Fig. 2.

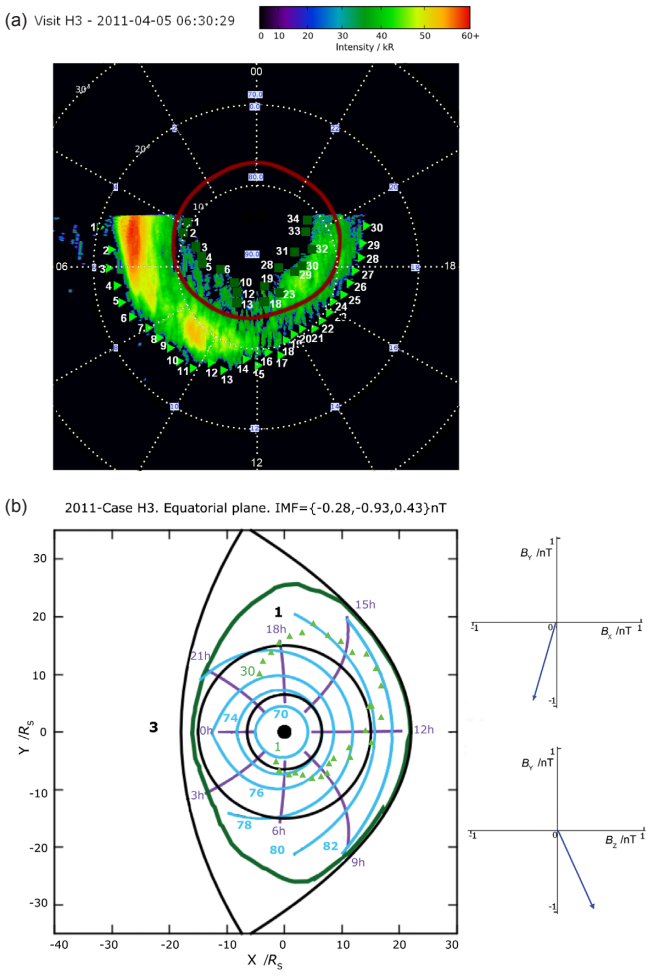

Figure 4. HST image and equatorial mapping for visit H3, in the same format as Fig. 2.

transit time across the magnetosheath to the subsolar magnetopause, and the one-way Alfvénic propagation time along high-latitude field lines from the magnetopause to the dayside ionosphere. Despite Cassini's location in the solar wind, the upstream plasma parameters in general remain unknown due to limitations in the plasma ion instrument field of view. For simplicity therefore, we assume intermediate solar wind conditions throughout, corresponding to a solar wind speed of $\sim 450\,\mathrm{km\,s^{-1}}$ and a dynamic pressure of ~ 0.03 nPa (e.g. Arridge et al., 2006). An exception is made for visit H4, however, which as noted above exhibits a "disturbed" auroral morphology indicative of magnetospheric compression, for which we assume a higher dynamic pressure of ~ 0.08 nPa. To determine the above propagation times, we have then

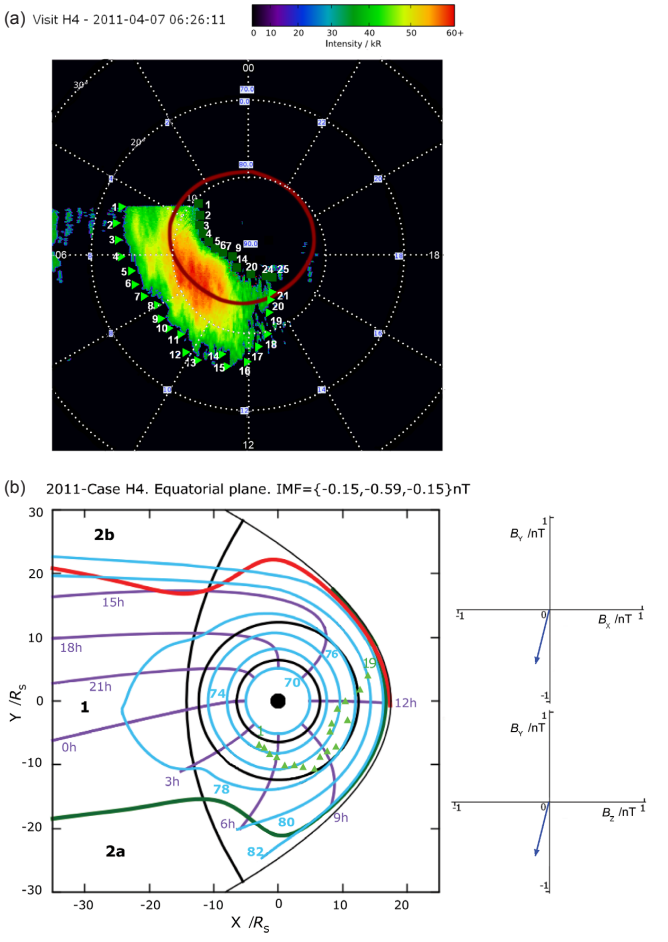

Figure 5. (a) HST image for visit H4, in the same format as Fig. 2. **(b)** Close-up of the near-planet equatorial magnetosphere in a format similar to Fig. 2b. The green and red lines mark the boundaries between closed lines (region 1), and open lines mapping to the northern (region 2a) and southern (region 2b) ionospheres, respectively.

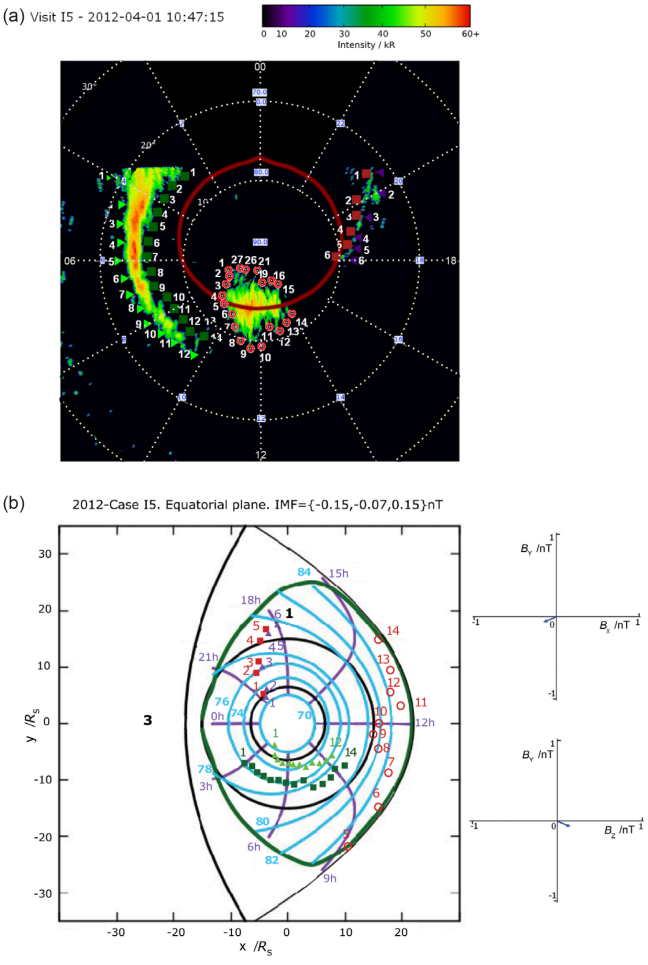

Figure 6. HST image and equatorial mapping for visit I5, in the same format as Fig. 2.

employed the bow shock and magnetopause models of Masters et al. (2008) and Kanani et al. (2010), respectively, parameterised by the solar wind dynamic pressure, together with the formulation of Khan and Cowley (1999) for the transit time across the magnetosheath. For the Alfvénic propagation to the ionosphere we have used a typical constant value of 30 min. The total lag times (t_1) for each image are given in column 4 of Table 1, and have values ∼ 1–2 h.

The IMF that influences the state of the dayside auroras at any time is not just the instantaneous lagged value, however, but the field over a significant prior period. Here we have taken this interval to extend 3 h prior to the minimum lag time, such that the maximum lag employed is ($t_2 = t_1 + 3$ h), given in column 5 of Table 1. The IMF data are thus averaged over the interval between times t_2 and t_1 prior to the centred Saturn time of each image as shown by the pink bands in Fig. 1. Given that magnetohydrodynamic models of the magnetosheath show that the flow speed over the magnetopause reaches a significant fraction of the upstream solar wind speed by the dawn–dusk meridian (e.g. Desroche et al., 2013), use of a typical solar wind speed to determine propagation times in the extended magnetosheath is reasonable. At typical flow speeds of $\sim 450\,\mathrm{km\,s^{-1}}$, therefore, the magnetosheath plasma outside the magnetosphere travels $\sim 80\,R_S$ in a 3 h interval, thus reaching distances down-tail from the planet after first contact at the nose that are ∼ 3 times the subsolar distance (typically $\sim 20\,R_S$). Our averages thus characterise the IMF concurrently interacting with the magnetosphere over a significant volume of the near-planet system, as seems appropriate.

The mean values of the three field components in KSM coordinates, together with the RMS deviations about them, are shown in columns 6–11 of Table 1. It is again seen that the image set contains a range of concurrent IMF conditions, in particular four with positive mean IMF B_z, likely to be conducive of open-flux production at Saturn's magnetopause, and four with negative mean IMF B_z, which likely is not. It

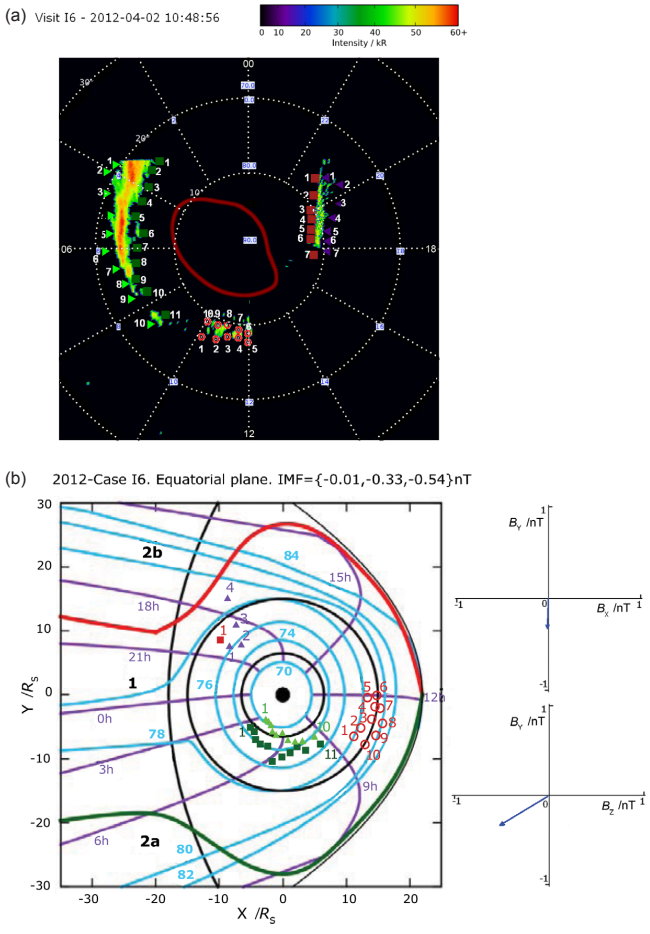

Figure 7. HST image and equatorial mapping for visit I6, in the same format as Fig. 5.

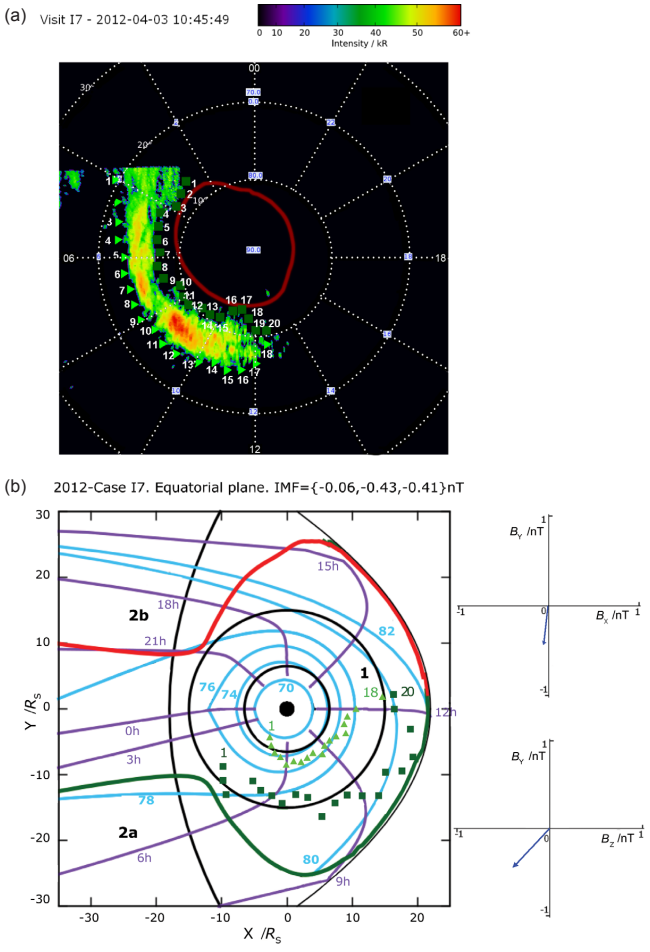

Figure 8. HST image and equatorial mapping for visit I7, in the same format as Fig. 5.

can also be seen that the RMS deviations about the means are generally rather smaller than the means themselves, such that the IMF components are not greatly variable about the mean values in the table. The only case in which the RMS deviation of the IMF B_z component (slightly) exceeds the mean, for example, occurs for visit H4. In addition, examination of the Cassini data in Fig. 1 shows that the mean values are not sensitively dependent on the exact interval employed to derive them. The mean IMF component values are then those used in the magnetic modelling described in the next section, and are the values referred to in all subsequent discussion.

3 Magnetic modelling results

The present study employs the modified magnetospheric magnetic field model discussed by Belenkaya et al. (2013), in which the internal field of the planet is taken to consist of dipole, quadrupole, and octupole terms in accordance with the results of Burton et al. (2010), while the ionospheric surface of maximum auroral emission is taken to be an axial spheroid 1100 km above the 1 bar reference surface, as employed in the HST image projections described above. As indicated in Sect. 1, current systems in the model represent the effect of the ring current and the tail currents within the magnetosphere, while shielding currents flow on the magnetopause, assumed to be a paraboloid of revolution about the KSM x axis, that fully contain the magnetic flux inside the boundary. To this is added a fraction of the mean IMF that is taken to penetrate inside the boundary, as will be discussed further below. Additional details may be found in Belenkaya et al. (2013), and in the references cited in Sect. 1. We note that the main perturbation fields not included in the model are those associated with magnetosphere–ionosphere field-aligned coupling currents produced by plasma sub-corotation (e.g. Cowley and Bunce, 2002; Cowley et al., 2004, 2005), and those associated with the "planetary period oscillations" (e.g. Andrews et al., 2010), that are of similar order. From simple estimates based on observed azimuthal fields, the azimuthal deflections of the field lines between the ionosphere and the equatorial plane associated with these systems are

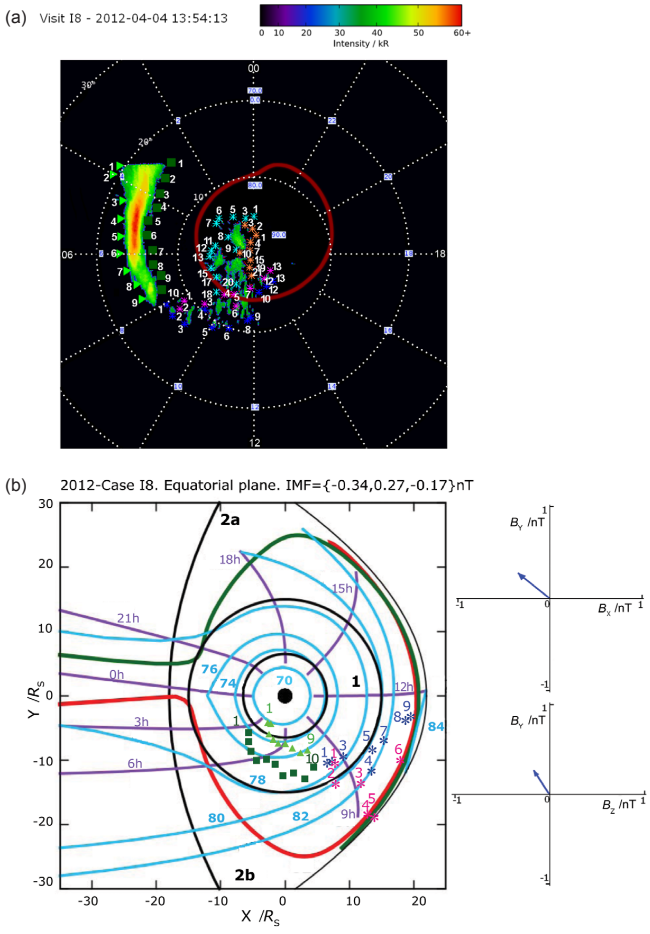

Figure 9. HST image and equatorial mapping for visit I8, in a similar format to Fig. 5. Patchy emissions in the pre-noon sector are now marked by blue (equatorward) and purple (poleward) asterisks.

negligible, by a few degrees or less, inside radial distances of $\sim 10\,R_S$, but may rise to of the order of $\sim 10°$ in the outer dayside magnetosphere beyond. This is not a major effect, however, particularly when mapping longitudinally elongated auroral structures. The planetary period oscillations are also associated with latitudinal oscillations of the aurora and radial oscillations of the plasma within the near-equatorial magnetosphere. However, the oscillation amplitude is only of the order of $\sim 1°$ latitude for the aurora (e.g. Nichols et al., 2010), and $\sim 1\,R_S$ in radial distance for the equatorial plasma in the outer magnetosphere (e.g. Clarke et al., 2010), such that neglect of these effects will not significantly affect the conclusions of this study.

Some of the parameters describing the model, such as the radial distance to the magnetopause, clearly depend on the solar wind dynamic pressure, which, as indicated in Sect. 2, remains in general unknown. Model parameters corresponding to low dynamic pressures of ~ 0.01 nPa and an expanded subsolar magnetopause at $\sim 28\,R_S$ appropriate to Cassini Saturn orbit insertion conditions have been derived by Alexeev et al. (2006), while parameters corresponding to high dynamic pressures of ~ 0.08 nPa and a compressed subsolar magnetopause at $\sim 17.5\,R_S$ appropriate to the Pioneer–11 flyby have been derived by Belenkaya et al. (2006a). However, in view of the unknown dynamic pressure conditions prevailing during the intervals examined here we use model parameters throughout derived by Belenkaya et al. (2008) that correspond to intermediate dynamic pressures of ~ 0.03 nPa and an intermediate subsolar magnetopause at $\sim 22\,R_S$. The latter distance corresponds to the most probable subsolar magnetopause radius found in the study of Cassini magnetopause data by Achilleos et al. (2008). An exception is made for visit H4, however, for which we employ the above "compressed" model in view of the auroral conditions prevailing, as discussed in Sect. 2. The specific parameters employed for the "intermediate" (compressed) cases are as follows (see Belenkaya et al., 2008, 2013, and references therein): (a) a radial distance to the subsolar magnetopause of 22 R_S (17.5 R_S), (b) inner and outer edges of the ring current at 6.5 (also 6.5) and 15 R_S (12.5 R_S), respectively, (c) a field strength at the outer edge of the ring current of 3.0 nT (3.62 nT), (d) a distance to the inner edge of the tail current sheet of 18 R_S (14 R_S), and (e) a field at the inner edge of the tail current sheet of 7 nT (8.7 nT). With regard to the coefficient of fractional penetration of the IMF vector into the magnetosphere, we note that empirical values determined for Earth lie typically in the range ~ 0.2–0.4 (e.g. Cowley and Hughes, 1983; Petrukovich, 2011). The value appropriate to Saturn has yet to be established by direct measurement, but on the basis of the results, for example, of Badman et al. (2005) discussed in Sect. 1, the value has been taken here to have a similar value of 0.2, at the low end of the above range. It was shown previously by Belenkaya et al. (2013), and will be confirmed below, that the resulting models provide a realistic estimate of the open flux within the Saturn system, judging from comparisons with the dark "polar cap" region bounded by the aurora. Magnetic mapping within the model is then derived by Runge–Kutta integration of the usual field line equations.

As indicated above, the Saturn paraboloid model has previously been successfully employed to model the magnetic field observations during Cassini Saturn orbit insertion under expanded magnetospheric conditions (Alexeev et al., 2006), as well as Pioneer–11 flyby data under compressed conditions (Belenkaya et al., 2006a). The intermediate model above then corresponds to intermediate parameters that incorporate an accurate model of the internal field of the planet (Burton et al., 2010), a model of the magnetopause appropriate to intermediate solar wind dynamic pressures (Arridge et al., 2006; Kanani et al., 2010; Achilleos et al., 2008), and a ring-current model based on Voyager and Cassini observations (Connerney et al., 1983; Bunce et al., 2007). As noted above, the model also yields realistic estimates of the amount of open flux in the system, when compared with auroral images (see e.g. Belenkaya et al., 2007, 2008, 2010, 2011,

2013). However, to investigate the sensitivity of the results to the detailed choice of model parameters, we have examined how the field line mapping from a few randomly chosen auroral boundary points in the HST images varies as the model parameters are changed over reasonable ranges, focusing on the ring-current parameters and the IMF penetration factor for a subsolar magnetopause position fixed at 22 R_S. Specifically, relative to intermediate model values we have varied the outer radius of the ring current by ± 1 R_S (i.e. between 14 and 16 R_S), its field strength parameter by ± 25 % (i.e. between 2.25 and 3.75 nT), and the IMF penetration parameter by a factor of two in either direction (i.e. between 0.1 and 0.4). The mapped coordinates in the equatorial plane were found to vary by ~ 0.5 R_S or less over the full range of these variations, showing that the mappings discussed below are not sensitively dependent on the specific model parameter choices.

Results for visit H1, for which the IMF is directed northward, are shown in Fig. 2b, where we show a view of the KSM equatorial plane with the Sun (x direction) to the right, and dusk (y direction) upward. The mean KSM IMF vector employed is indicated (to 2 decimal places) at the top of the figure, and is illustrated by the blue arrows to the right of the plot, which show the vector projected into the KSM x–y (upper plot) and y–z (lower plot) planes. As in all similar figures, the outer black line to the right shows the model magnetopause, that to the left shows the inner edge of the tail current, while the two black circles show the boundaries of the model ring current. The blue and violet lines then show lines of constant latitude and LT, respectively, mapped from the northern ionosphere to the equator as marked (2° intervals of latitude starting at 70° and 3 h intervals of LT). The solid green curve shows the boundary between closed field lines (region 1), and interplanetary field lines within the magnetosphere (region 3). Open field lines (potentially region 2) do not cross the equatorial plane for northward IMF.

The coloured symbols in Fig. 2b then show the mapped positions in the equatorial plane corresponding to the regions of auroral emission shown in Fig. 2a. It can first be seen that the segment of the dawn arc that is visible in the images, marked by the numbered light green triangles and dark green squares, maps between the inner edge and the centre of the model ring current in the dawn sector (only first and last numbers are indicated in Fig. 2b). The near-noon spot, however, shown by the open red circles, is seen to straddle the open–closed field boundary in Fig. 2a, and correspondingly maps into the pre-noon outer magnetosphere and magnetopause region in Fig. 2b. Those points on open field lines in Fig. 2a do not appear in Fig. 2b. Similarly, the points on the equatorward boundary of the dusk arc shown by the violet triangles generally map into the outer magnetosphere just beyond the ring current in Fig. 2b (except for points 1 and 2), while the points on the poleward boundary, again on open field lines (apart from anomalous point 10 shown by the brown square), do not appear in Fig. 2b. This arc is thus mapped into the outer magnetosphere and magnetopause region in the dusk sector.

The equatorial projection for visit H2 is shown in the same format in Fig. 3b, where the field structure is similar to that for visit H1 due to the similar mean northward IMF field components. In this case the equatorward edge of the dawn arc extends approximately along a noon–midnight direction from near the inner edge of the model ring current at dawn, similar to visit H1, towards its centre in the pre-noon sector. The poleward boundary of the emission, extending to higher latitudes than for H1, now lies in the outer magnetosphere in the pre-noon and dawn sector, but approaches and extends across the boundary of open field lines (near dark green square number 5) beyond the dawn meridian. The near-noon spot again straddles the open–closed boundary, with the boundary points on closed field lines mapping to the pre-noon outer magnetosphere near the magnetopause.

For visit H3 shown in Fig. 4b, however, for which the mean IMF was again northward but much stronger in all three KSM components than for visits H1 and H2, we find a continuous band of emission extending across the noon sector from beyond the dawn meridian on one side to beyond dusk on the other. As in previous cases, the equatorward edge of the emission lies near the inner edge of the model ring current near dawn, extends outward into the central ring current in the pre-noon sector, and then moves into the outer magnetosphere near the magnetopause in the post-noon sector, before moving back into the ring current post-dusk. The poleward edge of the emission then lies consistently on open field lines, and thus does not appear in the equatorial projection. It is notable, however, that the open–closed boundary lies near the poleward boundary of the emission in the pre-noon sector, but nearer to the equatorward boundary post-noon.

For visit H4 the mean IMF was directed southward (though somewhat variable), such that the structure of the equatorial field shown in Fig. 5b is different to that for the earlier cases in which the mean field was northward. In this case closed field lines (region 1) extend down the central tail to much larger distances than for northward IMF, bounded by the red and green lines. These are flanked by open field lines passing through the equatorial magnetosphere from the northern ionosphere in region 2a on the dawn side, and from the southern ionosphere in region 2b on the dusk side, for this polarity of IMF B_y (see, e.g. Belenkaya et al., 2013). We also recall from above that these results have been computed using the compressed magnetosphere model in this case, on the basis of the unusual morphology exhibited by the dawn auroras. It can be seen that the equatorward boundary of these emissions again maps near the inner ring current close to dawn, moves outward to the outer ring current pre-noon and then to the magnetopause post-noon as the emission crosses the open–closed boundary in Fig. 5a (after green triangle numbered 19). The remaining points, including all those on the poleward border, lie in the model region of open field lines, and pass across the magnetopause without crossing the

equatorial plane. Physically, however, the evident spatial homogeneity of the observed emissions, effectively bisected by the model open–closed boundary, indicates that it is unlikely that they originate from such diverse spatial locations. Instead, as discussed above, the steady-state model may overestimate the amount of open flux in the system at this time as a result of rapid time-dependent reconnection of open flux in the tail resulting from magnetospheric compression (Cowley et al., 2005). In that case the open–closed boundary may lie poleward of that indicated in the figure, certainly in the dawn sector.

Turning now to the images obtained during the 2012 HST campaign, the first of these for visit I5 is again for northward IMF, and has an auroral morphology with some similarities to H1. Specifically, the dawn arc is narrow in latitudinal extent, and maps in Fig. 6b between the inner edge and near the centre of the ring current on closed field lines, similar to visit H1. The near-noon spot again straddles the open–closed boundary with its equatorward portion mapping mainly to the outer magnetosphere just inside the dayside magnetopause, but is now located more centrally near to noon between ∼ 09:00 and ∼ 14:00 LT, rather than in the pre-noon sector as for visits H1 and H2. This may reflect the near-zero IMF B_y in the present case, rather than the positive B_y in the latter two cases. The dusk arc marked by the brown squares and violet triangles is unlike the dusk emission for H1, however, being latitudinally narrow, confined to LTs past the dusk meridian, and lying nearly wholly on closed field lines between the open–closed boundary near dusk and the inner edge of the ring current (similar to the latitude of the dawn arc) at later LTs. Point 6 on the poleward border marked by the brown squares lies just on open field lines and does not appear in the equatorial view.

For visit I6 the IMF had strong negative B_y and B_z components, with a consequent equatorial field structure in Fig. 7b that is similar to that for H4 in Fig. 5b. The dawn arc is once more narrow in latitudinal extent, and as in previous such cases, for visits H1 and I5 (both for northward IMF), maps between the inner edge of the model ring current and its centre, as shown by the green triangles and squares. The pre-noon patch of emission shown by the red circles then forms a longitudinal band straddling the outer boundary of the ring current, unlike the near-noon emissions for northward IMF in visits H1, H2, and I5, which straddle the open–closed boundary and hence map principally to the outer magnetosphere beyond the ring current and to the magnetopause. This result reinforces the suggestion in Sect. 2 that these emissions instead represent a patchy continuation of the dawn arc, located well away from the open–closed boundary in Fig. 7a. The dusk arc then has similar properties to that observed during visit I5 (for northward IMF), being latitudinally narrow and located wholly on closed field lines past the dusk meridian, stretching in the equatorial plane from deep within the dusk tail region, to inside the ring-current region in the pre-midnight sector as seen in Fig. 7b.

Visit I7 again has strong negative IMF B_y and B_z components, with a latitudinally broad dawn arc of variable intensity extending just past the noon meridian, and no separate noon spots or dusk emissions. As in other cases, the equatorward boundary of the dawn arc maps in Fig. 8b from the inner edge of the ring current in the dawn sector towards its centre near the noon meridian. The poleward boundary then maps near the outer edge of the ring current in the dawn sector, moving outwards into the outer magnetosphere and the vicinity of the magnetopause in the pre-noon sector. The emission thus lies wholly on closed field lines in the dawn and dayside sectors.

The IMF for visit I8 then has somewhat weaker positive B_y and negative B_z IMF components, and shows a narrow dawn arc, structured higher-latitude emissions in the pre-noon sector, and a very high latitude spot on the dawn side of the noon–midnight meridian extending close to the pole. As shown in Fig. 9b by the green triangles and squares, the dawn arc once more maps between the inner edge and centre of the model ring current in the dawn sector, moving outwards post-dawn and extending into the patchy band of emission mapping to the outer ring current and outer magnetosphere in the pre-noon sector shown by the dark blue and purple asterisks. The high-latitude emissions are then located principally on open field lines, and map in the equatorial plane to the dusk tail at large distances from the planet.

4 Auroral source locations

We now summarise and discuss the results shown in Figs. 2–9. With regard to the structure of the model field and its dependence on the IMF, we note that the results largely follow those described previously by Belenkaya et al. (2013). For northward IMF, the boundary between open and closed field lines lies in the northern ionosphere at ∼ 84° near noon and ∼ 77° near midnight (Figs. 2a–4a and 6a), while the boundary between closed and interplanetary field lines in the nightside equatorial plane lies at radial distances between ∼ 14 and ∼ 16 R_S down-tail (Figs. 2b–4b and 6b), almost independent of the other IMF components. For southward IMF the open–closed boundary still lies at ∼ 84° near noon, but is variably contracted near midnight to ∼ 79–85° depending on the magnitude of IMF B_z, and also shows significant dawn–dusk displacements depending on IMF B_y (Figs. 5a and 7a–9a). Correspondingly, the boundary of closed field lines in the equatorial plane in these cases extends down-tail to variable distances, flanked on either side by open-flux tubes mapping to either of the two polar ionospheres depending on the sign of IMF B_y. We note that these IMF-dependent features in the nightside model field appear to occur closer to the planet than indicated by Cassini data, which instead suggest the usual presence of closed flux to distances of a few tens of Saturn radii down-tail (e.g. Jackman and Arridge, 2011; Kellett et al., 2011), though intermittent reconnection

signatures such as tailward-travelling plasmoids are observed at distances beyond $\sim 30\,R_S$ (e.g. Jackman et al., 2011, and references therein). However, the mappings of principal interest here are of the dayside aurora into the dayside magnetosphere, where the magnetospheric field lines are confined by the currents on the dayside magnetopause rather than being stretched out to significant distances by the nightside currents in the tail, and hence being subject to somewhat less uncertainty.

Turning then to the mapping results, it can first be seen that the equatorward edge of the dawn arc maps consistently near the inner edge of the model ring current at radial distances of ~ 7–$8\,R_S$ near the dawn meridian, extending outwards towards the centre of the model ring current at $\sim 10\,R_S$ in the pre-noon sector. These distances correspond to the inner region of hot ions and electrons in Saturn's magnetosphere, where we note that the ring current at smaller radial distances is carried mainly by warm plasma originating from Enceladus (e.g. Kellett et al., 2011). For the four cases of latitudinally narrow arcs in this study (for visits H1, I5, I6, and I8), the outer boundary then maps typically near the centre of the ring current at a radial distance of $\sim 10\,R_S$. We note that of these four cases, two occur for positive mean IMF B_z (H1 and I5) and two for negative (I6 and I8), while similarly two occur for positive mean IMF B_y (H1 and I8) and two for negative (I5 and I6). The narrow-arc feature can thus occur for either sign of these two field components.

For the remaining cases of latitudinally broader dawn arcs, the poleward boundary maps to the outer magnetosphere beyond the ring-current region (H2, and I7 in the pre-noon sector), or close to the magnetopause boundary itself (H3 in the pre-noon sector). The only apparent exception occurs for visit H4, where as previously noted the dawn emissions extend continuously across the model open–closed boundary, an occurrence we attribute on the basis of past evidence to time-dependence under disturbed (compressed magnetosphere) conditions. We again note that of these four cases, two occur for positive mean IMF B_z (H2 and H3) and two for negative (H4 and I7), while one occurs for positive mean IMF B_y (H2) and three for negative (H3, H4, and I7), such that the broader-arc feature can also occur for either sign of these two field components. Allowing the apparent exception of visit H4 for the above reasons, we thus conclude that the dawn arc appears to be a wholly closed field line phenomenon associated with the dawn ring current and outer magnetosphere, that is, unresponsive in its gross features to the concurrent value of the IMF. This conclusion is in agreement with the corresponding discussion of Meredith et al. (2014). Instead, we suppose that its variations may be related more to nightside phenomena that inject hot plasma into the inner region via dawn (e.g. Mitchell et al., 2009b), thus related to the IMF only over longer timescales. The emissions may be related to field-aligned coupling currents due to plasma pressure gradients and/or flow shears associated with corotation breakdown in this region (e.g. Cowley, 2000; Cowley and Bunce, 2003; Cowley et al., 2004). However, it remains unclear why these auroras terminate in the pre-noon to noon sector, and do not extend significantly into the post-noon hours, at least not at intensities comparable to those on the dawn side (the apparent exception of visit H3 will be discussed below).

Turning now to the separate emissions near to noon observed in a number of the images, we first of all conclude that for two of the cases, for visits I6 and I8, the emissions initially identified are most likely continuations into the noon sector of patchy dawn arc emissions, on the bases of their more arc-like rather than spot-like form, and the fact that they are found to map principally to the outer ring current and outer magnetosphere region (Figs. 7b and 9b). The other cases, for H1, H2, and I5, all straddle the model open–closed field boundary, thus mapping to the dayside outer magnetosphere and magnetopause region (Figs. 2b, 3b, and 6b). We further note that all three cases occur for northward IMF B_z, making a connection with dayside reconnection and open-flux production in the noon sector plausible, as also suggested by Meredith et al. (2014). In addition, the spots are centred pre-noon for H1 and H2, which may be connected with the positive IMF B_y prevailing, while the spot for I5, for which B_y is small and positive, is centred closer to noon.

The fourth case with IMF B_z positive is H3, for which no separate noon spot is evident, but rather a continuous band is observed that extends throughout the dusk sector. It is notable, however, that the emission is located principally equatorward of the model open–closed boundary in the pre-noon sector, discussed above in relation to the "dawn arc" emissions, while becoming centred poleward of the open–closed boundary in the post-noon sector. It thus seems reasonable to suppose that these post-noon emissions may be related to the noon spots that also straddle the boundary, but now with emissions appearing continuously from noon to dusk for the case of the strongest positive IMF B_z in the data set. We note that similar emissions are also seen for visit H1, though with a gap in this case between these and the noon spot in the post-noon sector, while only weak vestiges of such emissions appear to be present for H2, and none for I5. Overall, it seems reasonable to suppose on the basis of these results that these noon and post-noon high-latitude emissions for positive IMF B_z are related to magnetopause phenomena, likely reconnection and open-flux production. The emphasis on the noon and post-noon sector is taken to relate to the flow shear across the magnetopause between the anti-sunward flowing magnetosheath plasma on one side and the sub-corotating magnetospheric plasma on the other, which maximises on the dawn side of noon, tending to suppress reconnection, and minimises on the dusk side, which may thus be favoured (Desroche et al., 2013).

The auroras for visit I8 are of special interest, in uniquely within this data set showing a patch of emission well within the region of open field lines, principally on the dawn side of the noon–midnight meridian, lying poleward of patchy

auroras on closed field lines most probably associated with the dawn arc. We note that this case occurred for the largest IMF B_x component in this data set, as well as for positive B_y and negative B_z, the equivalent polar field structure for which condition has been discussed for the terrestrial case by Belenkaya (1998). The emissions are thus likely associated with the currents set up by "lobe reconnection" between interplanetary and open tail lobe field lines, equivalent to the "NBZ currents" that occur at Earth (see Fig. 6 of Blomberg et al., 2005 and Fig. 8 of Belenkaya et al., 2006b), as also suggested by Meredith et al. (2014). The preference for dawn in this case is likely related to the positive IMF B_y conditions prevailing.

Finally, in two cases, visits I5 and I6, narrow auroral arcs are observed in the post-dusk sector, located principally on closed field lines, which pass from higher latitudes $\sim 80°$ near dusk to lower latitudes similar to that of narrow dawn arcs at later LTs. Although only two examples are present, one occurs for positive IMF B_z (I5) and the other for negative (I6), thus not suggesting a strong dependence on at least this component of the IMF. The further evolution of these emissions with increasing LT cannot be pursued with this data set, however, due to the lack of observations at oval latitudes across the midnight sector.

5 Summary and conclusions

In this paper we have examined northern dayside UV auroral features observed during eight HST imaging intervals during the 2011 and 2012 Saturn campaigns, when the Cassini spacecraft was located in the solar wind just upstream from the bow shock. Lagged 3 h averages of the IMF have been used within the paraboloid model of Saturn's magnetic field to map the observed auroral structures into the magnetosphere in order to examine their region of origin, thus providing information about their generation mechanism. In a parallel study of these images, Meredith et al. (2014) discussed the IMF dependence of the auroral morphology, finding no strong response of the dawn arc emissions, but suggesting that the structured higher-latitude emissions observed for northward IMF in the noon–dusk sector are associated with reconnection-related dynamics and open-flux production at the dayside magnetopause. They also suggested that the very high latitude emissions observed in one case with southward IMF is associated with lobe reconnection on open field lines. The magnetic mapping results presented here are found to be in good agreement with these suggestions, showing specifically the following features.

a. The dawn arc auroras map generally to the region of closed field lines in the dawn to noon sector. The equatorward boundary maps in the equatorial plane consistently near the inner edge of the ring current at $\sim 7\,R_S$ radial distance in the dawn sector, moving outwards to $\sim 10\,R_S$ in the pre-noon sector, towards the centre of the ring current. For narrow dawn arcs, observed in half our cases and for both positive and negative IMF B_y and B_z, the poleward boundary then lies near the centre of the ring current, often terminating in structured emissions as it meets the equatorward boundary in the pre-noon sector. Meredith et al. (2013) have previously suggested that such structures within the dawn arc could be caused by ULF waves driven by drift-bounce resonance with hot ring-current water group ions, consistent with the mapped location determined here. The broader dawn arcs observed in the other half of our cases, also for both positive and negative IMF B_y and B_z, have outer boundaries extending variably from the outer ring current at $\sim 15\,R_S$ to the outer magnetosphere beyond, up to the magnetopause, terminating variously in both pre-noon and post-noon sectors. One apparently discrepant case in which these emissions continuously straddle the model open–closed boundary is suggested on the basis of previous results to be due to time-dependency resulting from rapid compression of the magnetosphere not reproduced in the model. Overall, these results suggest that dawn arc properties are not connected directly with the concurrent value of the IMF, but rather with nightside processes that result in hot plasma injection from the tail onto closed flux tubes in the dawn sector. The emissions may then result from field-aligned currents associated both with plasma pressure gradients and corotation breakdown, as well as direct precipitation of hot plasma into the ionosphere.

b. Patchy auroras that straddle the model open–closed field boundary in the noon-to-dusk sector are observed exclusively for four cases of positive IMF B_z and not for four cases of negative IMF B_z, but for both signs of IMF B_y. These emissions variously take the form of a near-noon spot with or without further emissions along the boundary at larger LTs pre-dusk, or, in the case of the largest positive IMF B_z in this data set, a continuous band of high-latitude emission between noon and the post-dusk sector. Since these emissions straddle the open–closed boundary, they map along model field lines to the outer magnetosphere close to the magnetopause, and onto adjacent open field lines. These results are consistent with the suggestion that these emissions are associated with reconnection phenomena and open-flux production at the dayside magnetopause, related to the similarly interpreted emissions observed in Cassini UVIS data at higher spatial resolution by Radioti et al. (2011, 2013) and Badman et al. (2013). The auroras are likely pro-

duced through field-aligned currents associated with related momentum exchange between the magnetosphere and magnetosheath, together possibly with precipitation of reconnection-heated plasma. Post-noon is presumed favoured over pre-noon due to the reduced plasma flow shear across the boundary that occurs in this sector (Desroche et al., 2013).

c. In one case for negative IMF B_z, together with stronger negative B_x and positive B_y, very high latitude patchy emissions occur in the dawn sector, that extend above patchy emissions in the pre-noon sector apparently related to the dawn arc. Model results indicate that these emissions lie wholly on open field lines, consistent with the suggestion that they are due to the field-aligned current system resulting from lobe reconnection. The preference for the dawn sector in this case may then relate to the positive IMF B_y conditions prevailing, giving rise to near-antiparallel fields at high latitudes in the dawn sector. The flow-shear effect is not expected to be of great significance under these high-latitude circumstances.

d. Narrow post-dusk arcs are observed in two of four images from the 2012 HST campaign, one each for positive and negative IMF B_z, noting that a more extended view of these LTs is then available compared with the 2011 campaign images due to the developing Saturn northern spring season. These occur principally on closed field lines that extend from higher to lower latitudes with increasing LT from dusk, but their possible connections with the dawn arcs at similar latitudes cannot be investigated here due to the lack of observations across midnight at oval latitudes.

Acknowledgements. Work at the Lomonosov Moscow State University, Skobeltsyn Institute of Nuclear Physics (SINP MSU), and the University of Leicester (UoL) was supported by RFBR (grant no. 12-02-92600-КО_a) and London Royal Society (JP080836) Joint Project funding. Work at the SINP MSU was also supported by RFBR grants no. 12-05-00219-a and no. 11-05-00894-a, and the European FP7 project IMPEx (no. 262863), while work at the UoL was supported by STFC grants ST/H002480/1 and ST/K001000/1. This work employs observations made with the NASA/ESA Hubble Space Telescope, obtained at the Space Telescope Science Institute, which is operated by AURA Inc for NASA.

Topical Editor C. Owen thanks C. S. Arridge and one anonymous referee for their help in evaluating this paper.

References

Achilleos, N., Arridge, C. S., Bertucci, C., Jackman, C. M., Dougherty, M. K., Khurana, K. K., and Russell, C. T.: Large-scale dynamics of Saturn's magnetopause, J. Geophys. Res., 113, A11209, doi:10.1029/2008JA013265, 2008.

Alexeev, I. I., Kalegaev, V. V., Belenkaya, E. S., Bobrovnikov, S. Y., Bunce, E. J., Cowley, S. W. H., and Nichols, J. D.: A global magnetic model of Saturn's magnetosphere, and a comparison with Cassini SOI data, Geophys. Res. Lett., 33, L08101, doi:10.1029/2006GL025896, 2006.

Andrews, D. J., Cowley, S. W. H., Dougherty, M. K., and Provan, G.: Magnetic field oscillations near the planetary period in Saturn's equatorial magnetosphere: Variation of amplitude and phase with radial distance and local time, J. Geophys. Res., 115, A04212, doi:10.1029/2009JA014729, 2010.

Arridge, C. S., Achilleos, N., Dougherty, M. K., Khurana, K. K., and Russell, C. T.: Modeling the size and shape of Saturn's magnetopause with variable dynamic pressure, J. Geophys. Res., 111, A11227, doi:10.1029/2005JA011574, 2006.

Badman, S. V., Bunce, E. J., Clarke, J. T., Cowley, S. W. H., Gérard, J.-C., Grodent, D., and Milan, S. E.: Open flux estimates in Saturn's magnetosphere during the January 2004 Cassini-HST campaign, and implications for reconnection rates, J. Geophys. Res., 110, A11216, doi:10.1029/2005JA011240, 2005.

Badman, S. V., Masters, A., Hasegawa, H., Fujimoto, M., Radioti, A., Grodent, D., Sergis, N., Dougherty, M. K., and Coates, A. J.: Bursty magnetic reconnection at Saturn's magnetopause, Geophys. Res. Lett., 40, 1027–1031, doi:10.1002/grl.50199, 2013.

Belenkaya, E. S.: Reconnection modes for near-radial IMF, J. Geophys. Res., 103, 41–47, 1998.

Belenkaya, E. S., Alexeev, I. I., Kalegaev, V. V., and Blokhina, M. S.: Definition of Saturn's magnetospheric model parameters for the Pioneer 11 flyby, Ann. Geophys., 24, 1145–1156, doi:10.5194/angeo-24-1145-2006, 2006a.

Belenkaya, E. S., Cowley, S. W. H., and Alexeev, I. I.: Saturn's aurora in the January 2004 events, Ann. Geophys., 24, 1649–1663, doi:10.5194/angeo-24-1649-2006, 2006b.

Belenkaya, E. S., Alexeev, I. I., Blokhina, M. S., Cowley, S. W. H., Badman, S. V., Kalegaev, V. V., and Grigoryan, M. S.: IMF dependence of the open-closed field line boundary in Saturn's ionosphere, and its relation to the UV auroral oval observed by the Hubble Space Telescope, Ann. Geophys., 25, 1215–1226, doi:10.5194/angeo-25-1215-2007, 2007.

Belenkaya, E. S., Cowley, S. W. H., Badman, S. V., Blokhina, M. S., and Kalegaev, V. V.: Dependence of the open-closed field line boundary in Saturn's ionosphere on both the IMF and solar wind dynamic pressure: comparison with the UV auroral oval observed by the HST, Ann. Geophys., 26, 159–166, doi:10.5194/angeo-26-159-2008, 2008.

Belenkaya, E. S., Alexeev, I. I., Blokhina, M. S., Bunce, E. J., Cowley, S. W. H., Nichols, J. D., Kalegaev, V. V., Petrov, V. G., and Provan, G.: IMF dependence of Saturn's auroras: modelling study of HST and Cassini data from 12–15 February 2008, Ann. Geophys., 28, 1559–1570, doi:10.5194/angeo-28-1559-2010, 2010.

Belenkaya, E. S., Cowley, S. W. H., Nichols, J. D., Blokhina, M. S., and Kalegaev, V. V.: Magnetospheric mapping of the dayside UV auroral oval at Saturn using simultaneous HST images, Cassini

IMF data, and a global magnetic field model, Ann. Geophys., 29, 1233–1246, doi:10.5194/angeo-29-1233-2011, 2011.

Belenkaya, E. S., Cowley, S. W. H., Kalegaev, V. V., Barinov, O. G., and Barinova, W. O.: Magnetic interconnection of Saturn's polar regions: comparison of modelling results with Hubble Space Telescope UV auroral images, Ann. Geophys., 31, 1447–1458, doi:10.5194/angeo-31-1447-2013, 2013.

Blomberg, L. G., Cumnock, J. A., Alexeev, I. I., Belenkaya, E. S., Bobrovnikov, S. Yu., and Kalegaev, V. V.: Transpolar aurora: time evolution, associated convection patterns, and a possible cause, Ann. Geophys., 23, 1917–1930, doi:10.5194/angeo-23-1917-2005, 2005.

Bunce, E. J., Cowley, S. W. H., Alexeev, I. I., Arridge, C. S., Dougherty, M. K., Nichols, J. D., and Russell, C. T.: Cassini observations of the variation of Saturn's ring current parameters with system size, J. Geophys. Res., 112, A10202, doi:10.1029/2007JA012275, 2007.

Burton, M. E., Dougherty, M. K., and Russell, C. T.: Saturn's internal planetary magnetic field, Geophys. Res. Lett., 37, L24105, doi:10.1029/2010GL045148, 2010.

Clarke, J. T., Gérard, J.-C., Grodent, D., Wannawichian, S., Gustin, J., Connerney, J., Crary, F., Dougherty, M., Kurth, W., Cowley, S. W. H., Bunce, E. J., Hill, T., and Kim, J.: Morphological differences between Saturn's ultraviolet aurorae and those of Earth and Jupiter, Nature, 433, 717–719, 2005.

Clarke, J. T., Nichols, J., Gerard, J.-C., Grodent, D., Hansen, K. C., Kurth, W., Gladstone, G. R., Duval, J., Wannawichian, S., Bunce, E., Cowley, S. W. H., Crary, F., Dougherty, M., Lamy, L., Mitchell, D., Pryor, W., Retherford, K., Stellard, T., Zieger, B., Zarka, P., and Cecconi, B.: response of Jupiter's and Saturn's auroral activity to the solar wind, J. Geophys. Res., 114, A05210, doi:10.1029/2008JA013694, 2009.

Clarke, K. E., Andrews, D. J., Arridge, C. S., Coates, A. J., and Cowley, S. W. H.: Magnetopause oscillations near the planetary period at Saturn: Occurrence, phase, and amplitude, J. Geophys. Res., 115, A08209, doi:10.1029/2009JA014745, 2010.

Connerney, J. E. P., Acuña, M. H., and Ness, N. F.: Currents in Saturn's magnetosphere, J. Geophys. Res., 88, 8779–8789, 1983.

Cowley, S. W. H.: Magnetospheric and ionospheric flow and the interplanetary magnetic field, in: The Physical Basis of the Ionosphere in the Solar-Terrestrial System, AGARD-CP-295, (4 1)–(4 14), 1981.

Cowley, S. W. H.: Magnetosphere-ionosphere interactions: A tutorial review, in: Magnetospheric Current Systems, edited by: Ohtani, S., Fujii, R., Hesse, M., and Lysak, R. L., Geophys. Monograph 118, AGU Publ., Washington, 91–106, 2000.

Cowley, S. W. H. and Bunce, E. J.: Corotation-driven magnetosphere-ionosphere coupling currents in Saturn's magnetosphere and their relation to the auroras, Ann. Geophys., 21, 1691–1707, doi:10.5194/angeo-21-1691-2003, 2003.

Cowley, S. W. H. and Hughes, W. J.: Observation of an IMF sector effect in the Y magnetic field component at geostationary orbit, Planet. Space Sci., 31, 73–90, 1983.

Cowley, S. W. H., Bunce, E. J., and Prangé, R.: Saturn's polar ionospheric flows and their relation to the main auroral oval, Ann. Geophys., 22, 1379–1394, doi:10.5194/angeo-22-1379-2004, 2004.

Cowley, S. W. H., Badman, S. V., Bunce, E. J., Clarke, J. T., Gérard, J.–C., Grodent, D., Jackman, C. M., Milan, S. E., and Yeoman, T. K.: Reconnection in a rotation-dominated magnetosphere and its relation to Saturn's auroral dynamics, J. Geophys. Res., 110, A02201, doi:10.1029/2004JA010796, 2005.

Desroche, M., Bagenal, F., Delamere, P. A., and Erkaev, N.: Conditions at the magnetopause of Saturn and implications for the solar wind interaction, J. Geophys. Res., 118, 3087–3095, doi:10.1002/jgra.50294, 2013.

Gérard, J.–C., Bonfond, B., Gustin, J., Grodent, D., Clarke, J. T., Bisikalo, D., and Shematovich, V.: Altitude of Saturn's aurora and its implications for the characteristic energy of precipitated electrons, Geophys. Res. Lett., 36, L02202, doi:10.1029/2008GL036554, 2009.

Grodent, D., Gérard, J.-C., Cowley, S. W. H., Bunce, E. J., and Clarke, J. T.: Variable morphology of Saturn's southern ultraviolet aurora, J. Geophys. Res., 110, A07215, doi:10.1029/2004JA010983, 2005.

Jackman, C. M. and Arridge, C. S.: Statistical properties of the magnetic field in the Kronian magnetotail lobes and current sheet, J. Geophys. Res., 116, A05224, doi:10.1029/2010JA015973, 2011.

Jackman, C. M., Achilleos, N., Bunce, E. J., Cowley, S. W. H., Dougherty, M. K., Jones, G. H., Milan, S. E., and Smith, E. J.: Interplanetary magnetic field at $\sim$9 AU during the declining phase of the solar cycle and its implications for Saturn's magnetospheric dynamics, J. Geophys. Res., 109, A11203, doi:10.1029/2004JA010614, 2004.

Jackman, C. M., Slavin, J. A., and Cowley, S. W. H.: Cassini observations of plasmoid structure and dynamics: Implications for the role of magnetic reconnection in magnetospheric circulation at Saturn, J. Geophys. Res., 116, A10212, doi:10.1029/2011JA016682, 2011.

Kanani, S. J., Arridge, C. S., Jones, G. H., Fazakerley, A. N., McAndrews, H. J., Sergis, N., Krimigis, S. M., Dougherty, M. K., Coates, A. J., Young, D. T., Hansen, K. C., and Krupp, N.: A new form of Saturn's magnetopause using a dynamic pressure balance model, based on in situ, multi-instrument Cassini measurements, J. Geophys. Res., 115, A06207, doi:10.1029/2009JA014262, 2010.

Kellett, S., Arridge, C. S., Bunce, E. J., Coates, A. J., Cowley, S. W. H., Dougherty, M. K., Persoon, A. M., Sergis, N., and Wilson, R. J.: Saturn's ring current: Local time dependence and temporal variability, J. Geophys. Res., 116, A05220, doi:10.1029/2010JA016216, 2011.

Khan, H. and Cowley, S. W. H.: Observations of the response time of high-latitude ionospheric convection to variations in the interplanetary magnetic field using EISCAT and IMP-8 data, Ann. Geophys., 17, 1306–1335, doi:10.1007/s00585-999-1306-8, 1999.

Krupp, N., Vasyliunas, V. M., Woch, J., Lagg, A., Khurana, K. K., Kivelson, M. G., Mauk, B. H., Roelof, E. C., Williams, D. J., Krimigis, S. M., Kurth, W. S., Frank, L. A., and Paterson, W. R.: The dynamics of the jovian magnetosphere, in: Saturn from Cassini-Huygens, edited by: Bagenal, F., Dowling, T. E., and McKinnon, W. B., Cambridge University Press, 617–638, 2004.

Masters, A., Achilleos, N., Dougherty, M. K., Slavin, J. A., Hospodarski, G. B., Arridge, C. S., and Coates, A. J.: An empirical model of Saturn's bow shock: Cassini observations of shock location and shape, J. Geophys. Res., 113, A10210, doi:10.1029/2008JA013276, 2008.

Masters, A., Eastwood, J. P., Swisdak, M., Thomsen, M. F., Russell, C. T., Sergis, N., Crary, F. J., Dougherty, M. K., Coates, A. J., and Krimigis, S. M.: The importance of plasma β conditions for magnetic reconnection at Saturn's magnetopause, Geophys. Res. Lett., 39, L08103, doi:10.1029/2012GL051372, 2012.

Meredith, C. J., Cowley, S. W. H., Hansen, K. C., Nichols, J. D., and Yeoman, T. K.: Simultaneous conjugate observations of small-scale structures in Saturn's dayside ultraviolet auroras – implications for physical origins, J. Geophys. Res., 118, 2244–2266, doi:10.1002/jgra.50270, 2013.

Meredith, C. J., Alexeev, I. I., Badman, S. V., Belenkaya, E. S., Cowley, S. W. H., Dougherty, M. K., Kalegaev, V. V., Lewis, G. R., and Nichols, J. D.: Saturn's dayside ultraviolet auroras: Evidence for morphological dependence on the direction of the upstream interplanetary magnetic field, J. Geophys. Res., 119, 1994–2008, doi:10.1002/2013JA019598, 2014.

Mitchell, D. G., Carbary, J. F., Cowley, S. W. H., Hill, T. W., and Zarka, P.: The dynamics of Saturn's magnetosphere, in: Saturn from Cassini-Huygens, edited by: Dougherty, M. K., Esposito, L. W., and Krimigis, S. M., Springer Science & Business Media, 257–279, 2009a.

Mitchell, D. G., Krimigis, S. M., Paranicas, C., Brandt, P. C., Carbary, J. F., Roelof, E. C., Kurth, W. S., Gurnett, D. A., Clarke, J. T., Nichols, J. D., Gérard, J.–C., Grodent, D. C., Dougherty, M. K., and Pryor, W. R.: Recurrent energization of plasma in the midnight-to-dawn quadrant of Saturn's magnetosphere, and its relationship to auroral UV and radio, Planet. Space Sci., 57, 1732–1742, 2009b.

Nichols, J. D., Cowley, S. W. H., and Lamy, L.: Dawn-dusk oscillation of Saturn's conjugate auroral ovals, Geophys. Res. Lett., 37, L24102, doi:10.1029/2010GL045818, 2010.

Owen, C. J. and Cowley, S. W. H.: A note on current sheet stress balance in the geomagnetic tail for asymmetrical tail lobe plasma conditions, Planet. Space Sci., 35, 467–474, 1987.

Petrukovich, A. A.: Origins of plasma sheet B_y, J. Geophys. Res., 116, A07217, doi:10.1029/2010JA016386, 2011.

Prangé, R., Pallier, L., Hansen, K. C., Howard, R., Vourlidas, A., Courtin, R., and Parkinson, C.: An interplanetary shock traced by planetary auroral storms from the Sun to Saturn, Nature, 432, 78–81, 2004.

Radioti, A., Grodent, D., Gérard, J.-C., Milan, S. E., Bonfond, B., Gustin, J., and Pryor, W.: Bifurcations of the main auroral ring at Saturn: Ionospheric signatures of consecutive reconnection events at the magnetopause, J. Geophys. Res., 116, A11209, doi:10.1029/2011JA016661, 2011.

Radioti, A., Grodent, D., Gérard, J.-C., Bonfond, B., Gustin, J., Pryor, W., Jasinski, J. M., and Arridge, C. S.: Auroral signatures of multiple magnetopause reconnection at Saturn, Geophys. Res. Lett., 40, 4498–4502, doi:10.1002/grl.50889, 2013.

Swisdak, M., Rogers, B. N., Drake, J. F., and Shay, M. A.: Diamagnetic suppression of component magnetic reconnection at the magnetopause, J. Geophys. Res., 108, 1218, doi:10.1029/2002JA009726, 2003.